Author's Accepted Manuscript

Spark plasma sintered Al-based composites reinforced with BN nanosheets exfoliated under ball milling in ethylene glycol

Khabib U. Yusupov, Shakti Corthay, Andrey V. Bondarev, Andrey M. Kovalskii, Andrey T. Matveev, Dmitry Arkhipov, Dmitri V. Golberg, Dmitry V. Shtansky

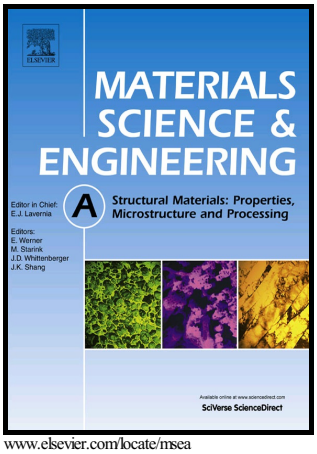

www.elsevier.com/locate/msea

PII: S0921-5093(18)31719-2
DOI: https://doi.org/10.1016/j.msea.2018.12.040
Reference: MSA37312

To appear in: *Materials Science & Engineering A*

Received date: 19 November 2018
Revised date: 7 December 2018
Accepted date: 10 December 2018

Cite this article as: Khabib U. Yusupov, Shakti Corthay, Andrey V. Bondarev, Andrey M. Kovalskii, Andrey T. Matveev, Dmitry Arkhipov, Dmitri V. Golberg and Dmitry V. Shtansky, Spark plasma sintered Al-based composites reinforced with BN nanosheets exfoliated under ball milling in ethylene glycol, *Materials Science & Engineering A,* https://doi.org/10.1016/j.msea.2018.12.040

This is a PDF file of an unedited manuscript that has been accepted for publication. As a service to our customers we are providing this early version of the manuscript. The manuscript will undergo copyediting, typesetting, and review of the resulting galley proof before it is published in its final citable form. Please note that during the production process errors may be discovered which could affect the content, and all legal disclaimers that apply to the journal pertain.

ACCEPTED MANUSCRIPT

Spark plasma sintered Al-based composites reinforced with BN nanosheets exfoliated under ball milling in ethylene glycol

Khabib U. Yusupov[a,*], Shakti Corthay[a], Andrey V. Bondarev[a], Andrey M. Kovalskii[a], Andrey T. Matveev[a], Dmitry Arkhipov[a], Dmitri V. Golberg[b,c], Dmitry V. Shtansky[a,*]

[a]*National University of Science and Technology "MISIS" Leninsky prospect 4, Moscow 119049, Russian Federation*

[b]*Science and Engineering Faculty, Queensland University of Technology (QUT), 2nd George st., Brisbane, QLD 4000, Australia*

[c]*International Center for Materials Nanoarchitectonics (MANA), National Institute for Materials Science (NIMS), Namiki 1-1, Ibaraki 3050044, Japan*

E-mail addresses: khabibyusupov2014@gmail.com (K.U. Yusupov); shtansky@shs.misis.ru (D.V. Shtansky)

**Corresponding author:*

Accepted manuscript

Abstract

Herein we demonstrate the promise of hexagonal BN nanosheets (BNNSs) as fillers in metal matrix composites (MMCs). Al-based MMCs with 1, 5 and 10 wt.% of BNNSs were obtained by spark plasma sintering using BNNSs (approximately 300×600 nm^2 and 20-50 nm thick) exfoliated under ball milling in ethylene glycol. Particular attention was paid to the optimisation of ball milling process in various media to achieve a high yield of high-quality BNNSs. The resulting Al-BNNSs composites consisted of Al grains separated by BN layers with a widely varied width from 20 nm to 1-2 μm. Within these layers, individual *h*-BNNSs, approximately 5-10 nm thick and up to 200 nm long, were mostly oriented in parallel to the Al grain boundaries. The maximum tensile strength of 152 MPa was obtained for a sample with 1 wt.% of BNNSs, hereby demonstrating a 69% increase compared to pristine Al. Thorough structural investigation showed that Al grains and BN layers had exhibited strong cohesion to each other and withstood high applied loads. Using SEM and high-resolution TEM analysis of fractured surfaces direct experimental evidence of BNNSs involvement into the deformation process through taking over most of the load was obtained.

ACCEPTED MANUSCRIPT

Keywords:

Al-based composites; Ball milling; Spark plasma sintering; Microstructure; Tensile strength

1. Introduction

Metal matrix composites (MMCs) are attracting ever-growing interest in many fields due to functional combination of a ductile metal matrix and a tough reinforcing phase [1-3]. As a matrix material, aluminum (Al) is one of the most commonly used metals due to its lightweight, excellent corrosion resistance, high specific strength, decent paramagnetic characteristics, and good thermal properties [4-6]. Al-based MMCs are widely used in aerospace, automotive, and sport industries [7-9]. However, pure Al is soft. The mechanical properties of pristine Al (stiffness and ultimate tensile strength) are rather poor and further dramatically decrease when a material is heated to only a few hundred degrees [10]. Over the past few years various kinds of fillers; for example, carbon nanotubes (CNTs), graphene nanosheets, oxide, ceramic, metallic and glassy particles have been utilized as the reinforcing phases in Al-MMCs [11-17]. Due to attractive mechanical properties, BN nanostructures are superb reinforcing agents for lightweight MMCs. High-strength Al-based MMCs reinforced with BN nanostructures have recently been reviewed by Yamaguchi et al. [18]. Comparison of the mechanical properties of Al-based MMCs reinforced with different additives (CNTs, Al_2O_3, SiC, ZrO_2, metallic and glassy particles, BN micro- and nanostructures) have been obtained through different methods. These studies have indicated that the maximum tensile strength and the highest percentage of improvement (135%) are achieved via utilization of BNMPs due to the formation of more homogeneous and uniform morphologies within the ball-milled powder mixtures and, as a result, a good quality of the resultant spark-plasma sintering products [19]. The undoubtful advantage of Al-MMCs reinforced with BN structures is a particularly high strength (185% increase *vs* Al) at elevated temperatures (~500 ^{o}C). Composite materials based on Al containing only 5 wt.% of BN particles demonstrated the room-temperature tensile strength as high as 380 MPa, which is already comparable with the strength of some structural steels, but the reinforced MMCs are nearly three times lighter.

Accepted manuscript

ACCEPTED MANUSCRIPT

Using density functional theory (DFT) calculations it was demonstrated that active chemical edges of the graphene-like BN nanosheets (BNNSs) create strong chemical bonding between the fillers and a metal matrix, thereby ensuring critical shear stress in the GPa range [20,21]. Thus the regarded nanosheet morphology of BN nanostructures is of particular interest for strengthening of Al-based MMCs. The desired BNNSs can be obtained using different techniques, for example by sonicating or ball milling [22-26].

Herein a reactive ball milling process was utilized to obtain BNNSs. The ball milling experiments were carried out in different media (argon, isopropanol, ethylene glycol) by varying the diameter of milling balls (5, 7, and 9 mm) and milling time (from 20 min to 4 h) to control the milling process intensity. The successfully exfoliated BNNSs taken at the amount of 1, 5, and 10 wt.% were further utilized to produce Al-MMCs composites using Spark Plasma Sintering (SPS) method. The obtained samples were tensile tested at room temperature. The significant improvement in the tensile strength of MMCs (from 90 to 152 MPa) was achieved with only 1 wt.% of BNNSs additives.

2. Materials and methods

2.1 Raw materials

Commercially available hexagonal boron nitride (*h*-BN) from "Reachem" (Russian Federation) with an average particles size of 7-15 μm was utilized as a raw material for ball milling process. Aluminum powder of 99% purity with an average particles size of 12 μm was purchase from STREM Chemical Inc.

2.2 Fabrication of BNNSs

BNNSs were obtained *via* the reactive ball milling using a high energy ball mill mixer "Activator 2S". The ball milling was performed in a milling chamber (250 mm in diameter) filled either with argon gas or in the presence of liquid medium (isopropanol, ethylene glycol) at a constant rotation speed of 694 rpm and the BN powder/milling ball weight ratio of 0.025. The volume ratio of milling balls to vial was set as 1:3 [26]. In contrast to the commonly used ball

ACCEPTED MANUSCRIPT

milling mode, when the balls randomly move in space, in our case the processing was carried out by such a way that the milling balls moved along the periphery of the chamber in contact with the walls (Fig. 1). Under this regime, the BN particles were affected tangentially rather than normally as in the case of chaotic bombardment. This allowed us to obtain the desired sheet-like BN morphologies due to the occurrence of bursting stress between the layers of BN particles at the moment of the tangential collision with balls.

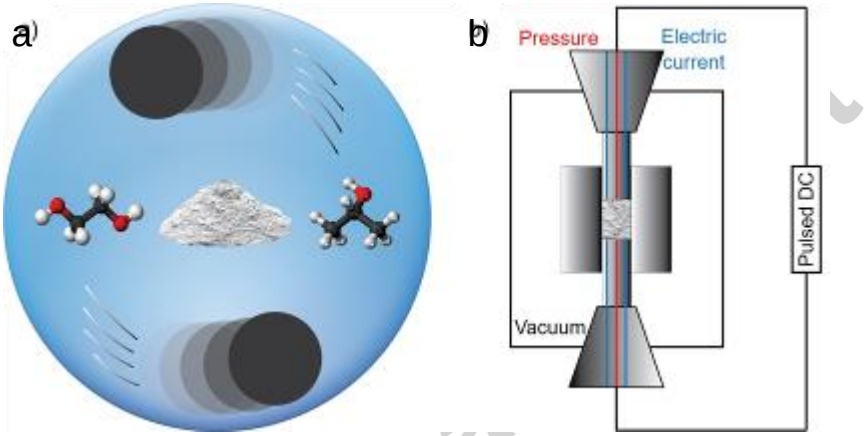

Fig. 1. Schematic representations of BNNSs exfoliation during ball milling in liquid medium (a) and Al-BNNSs composite fabrication *via* spark plasma sintering (b).

The ball milling regimes are summarized in Table 1. To establish the optimal ball milling mode, the following parameters were controlled: milling time was gradually decreased from 240 to 20 min, processing was carried out in different media (Ar, isopropanol, ethylene glycol), media to powder weight ratio was set to either 1:1 or 2:1, and ball milling was carried out using either a mixture of balls with diameterы of 5, 7 and 9 mm in equal proportion [27] or balls of a specific diameter (5, 7 or 9 mm). All experiments were performed sequentially: first, we set the optimal processing time of 20 min (samples A series), then the optimal isopropanol/BN powder weight ration (ξ=2:1) was established (samples B series), and, finally, the optimal ball diameter was experimentally selected (samples C series) to achieve the uniform BNNS size distribution.

2.3 Fabrication of Al-BNNSs composites

ACCEPTED MANUSCRIPT

Exfoliated BNNSs were first dried in a fume hood at 100 ^{o}C for 12 h, then mixed with isopropanol and further sonicated for 10 min. The BNNSs suspension was left untouched for 10 min to avoid its overheating. Then the BNNSs were magnetically mixed with Al powder and subjected to three consecutive sonications for 10 min at the rest intervals of 10 min. Finally, the Al-BNNSs mixtures were dried at 80 ^{o}C for 2 h to let the isopropanol evaporate. The Al-BNNS MMCs were fabricated by SPS using a LABOX 650 press (Sinter Land Inc., Japan). Vacuum sintering was carried out in a graphite die with an inner diameter of 30 mm under the following technological parameters: sintering temperature - 600 ^{o}C, sintering pressure - 35 kN, isothermal holding at the sintering temperature – 1 h.

Table 1 Ball milling regimes

Series	Sample	Milling parameters			
		Milling time, min	Medium	Medium to BN powder weight ratio, ξ	Ball diameter, mm
A	A1	240	Ar	-	Ball mixture*
	A2	20	Ar	-	Ball mixture
	B1	20	Isopropanol	1:1	Ball mixture
B	B2	20	Isopropanol	2:1	Ball mixture
	B3	20	Ethylene glycol	2:1	Ball mixture
	C1	20	Ethylene glycol	2:1	5
C	C2	20	Ethylene glycol	2:1	7
	C3	20	Ethylene glycol	2:1	9

* A mixture of balls with diameters of 5, 7 and 9 mm

2.4 Structural characterization

All as-fabricated materials (BNNSs, powder mixtures, and sintered samples) were studied *via* scanning electron microscopy (SEM), transmission electron microscopy (TEM), energy-dispersive X-ray spectroscopy (EDX), and X-ray diffraction (XRD).

The microstructures and chemical compositions were analyzed by a scanning electron microscope JSM F7600 (JEOL Ltd., Japan) equipped with a silicon drift EDX detector X-Max 80 mm. XRD patterns were recorded in the range of 25–140^{o} 2θ on a DIFRAY-401 diffractometer (Scientific Instruments) equipped with a position sensitive detector (Elion) using the Bragg–Brentano geometry and CrK_{α} radiation (k = 0.22897 nm). A linear X-ray source was operated at 25 kV and 4 mA. A JEM-2100 transmission electron microscope (JEOL) equipped

ACCEPTED MANUSCRIPT

with an X-Max 80 EDX detector (Oxford Instruments) was employed for fine structural analysis. The Al-BNNSs specimens for TEM investigations were prepared using PIPS II ion polishing system (Gatan). For structural investigations, the ball milled BN powders were ultrasonically deposited onto TEM grids in isopropanol.

2.5 Mechanical testing

The sintered samples were cut into strips, 230 mm^3, using a Secotom 50 precision cutting machine (Struers Inc., Taiwan) and further reshaped into special dumbbell-shaped specimens form using a Chmer GX-320L electric discharge cutting machine (Taiwan). The reshaped samples were subjected to tensile tests at a strain rate of 0.83×10^{-4} m/s until complete sample failure using a universal testing machine Shimadzu AG-X Series (Shimadzu Corp., Japan). The tests were carried out at room temperature at a maximum load of 20 kN.

3. Results and discussion

3.1 Optimisation of ball milling process

3.1.1 Processing time

Morphology of BN nanoparticles in dependence to the varied ball milling parameters is shown in Fig. 2. Additional SEM micrographs of the *h*-BN particles after ball milling are collected in Fig. S1. At the first step, the processing time was adjusted to obtain nanosized particles. After ball milling for 240 min the size of BN nanoparticles decreased from 7-15 μm to 50 nm (Fig. S1a) and did not change further while reducing the milling time to 20 min (Fig 2a). Since the minimum processing time is always desirable from a technological point of view, the milling time of 20 min was used in all further experiments.

3.1.2. Processing medium

Subsequent experiments were aimed at obtaining the sheet-like BN nanoparticle morphology. It is known that the density of processing medium can affect the shape of ball milled particles. Thus the processing medium was changed from argon to isopropanol (Iso) that

Accepted manuscript

has a density of ~0.79 g/m^3. SEM image of the *h*-BN particles (B1 sample) after ball milling in Iso (ξ=1:1) showed that the size of BN particles did not change compared to their processing in the Ar atmosphere (Fig. S1b). Once ξ parameter was changed to 2:1 (B2 sample), the shape of some fraction of BN particles changed from sphere-like to plate-like type (Fig. 2b). Note, however, that the yield of BNNSs was still small. To solve this problem the Iso medium was further replaced by ethylene glycol (EG), which has a higher density of 1.11 g/m^3. This led to a significant increase in BNNSs yield, i.e. almost all BN particles exhibited the sheet-like morphology, although the BNNSs size and thickness significantly differed (Fig. 2c). This was attributed to the use of a mixture of balls of various diameters, since the collision of balls of different sizes with BN particles led to the exfoliation of nanosheets of different sizes.

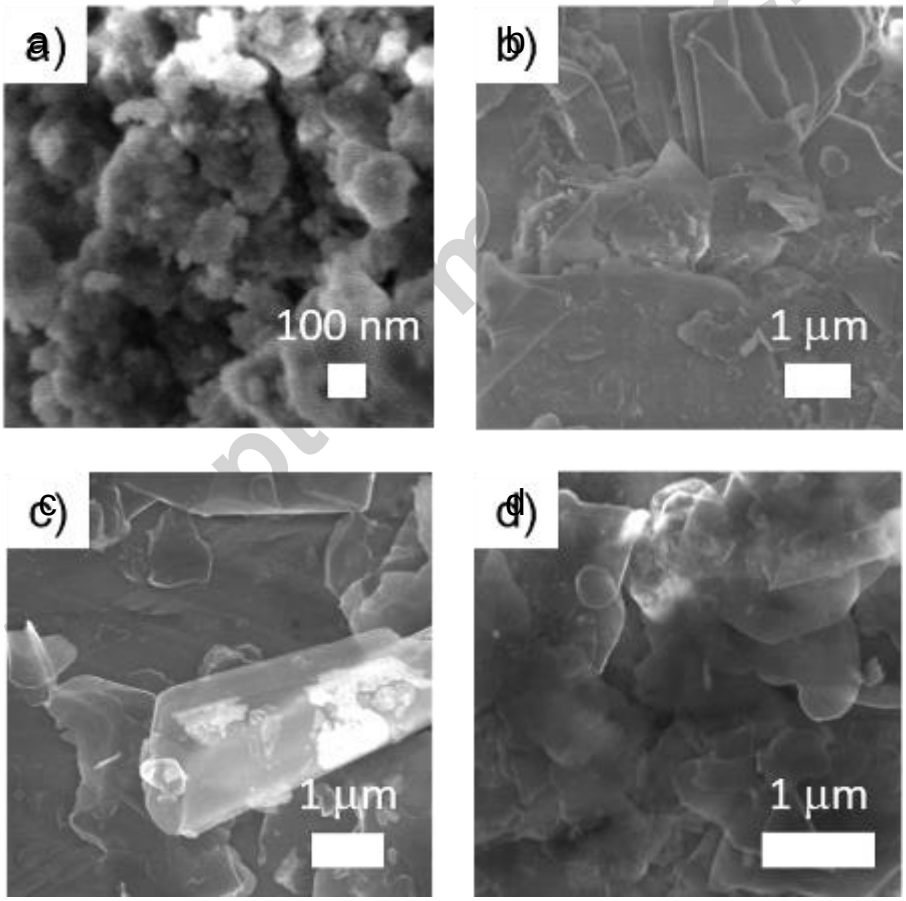

Fig. 2. SEM images of h-BN particles after ball milling for 20 min under the following conditions: Ar, ball mixture (a); isopropanol (ξ=2:1), ball mixture (b); ethylene glycol (ξ=2:1), ball mixture (c); ethylene glycol (ξ=2:1), 7 mm balls (d).

ACCEPTED MANUSCRIPT

3.1.3. Ball size

In subsequent experiments we utilized milling balls of a specific diameter, namely 5, 7 and 9 mm (Table 1, samples C1, C2 and C3, respectively). However, when processing was done with 5 and 9 mm balls, a weak degree of exfoliation and a larger size of final BNNSs were observed (Figure S1c and d). In contrast, the ball milling with 7 mm balls led to the formation of exfoliated BNNSs more uniform in size (Fig. 2d). This type of BNNSs was used for the preparation of Al/BN mixtures and their further spark plasma sintering.

Successful formation of BNNSs during the ball milling process can be explained as follows. Conventional ball milling in air does not lead to BNNSs flaking, whereas during processing in the liquid medium (Iso), a thin liquid layer is formed between the BN powder and milling balls. Since rotating balls mainly affect the medium rather than the BN particles themselves, a part of the ball kinetic energy is passed to the liquid medium and the BNNSs exfoliation occurs as a result of tangential forces applied to the BN particle surfaces. When using a denser medium (EG), the exfoliation yield is significantly increased thereby further confirming the proposed mechanism of BN nanosheet exfoliation.

3.2. Microstructure of exfoliated BNNSs

Microstructure of BNNSs obtained after ball milling and subsequently used as reinforcing component in the Al-BNNSs composites produced *via* SPS is shown in Fig. 3. It can be seen that during ball milling, the BN particles were laminated into individual nanosheets. BNNSs have an average size of 300×600 nm and a thickness of approximately 20-50 nm. HRTEM images revealed a characteristic interplanar spacing of 0.33 (side view) and 0.22 nm (plane view) for (002) and (100) planes, respectively (PDF card No. 45-0896). The results of EDS analysis presented in Fig. 3d indicate that the BNNSs are N-deficient. Note that in pure BN, used as a reference in the EDS method, deviation from stoichiometry did not exceed ± 0.5 at.%. Some of the BNNSs were densely populated with small nanoparticles (NPs), 1-4 nm in size (Fig. 3c). EDS analysis performed in the region containing NPs also detected the presence of a small amount of O, Cr, and Fe. Thus, these NPs appear to be metal oxide byproducts which formed during ball milling using steel balls. The XRD patterns of BNNSs before and after annealing in

Accepted manuscript

vacuum at 100 ^{o}C for 12 h are depicted in Fig. 3e. The full width at half maximum values of the BN peaks was rather small and did not change after the heat treatment. This result indicates that in contrast to the conventional ball milling process, which leads to a high degree of material deformation [28], the degree of BNNS imperfection is low.

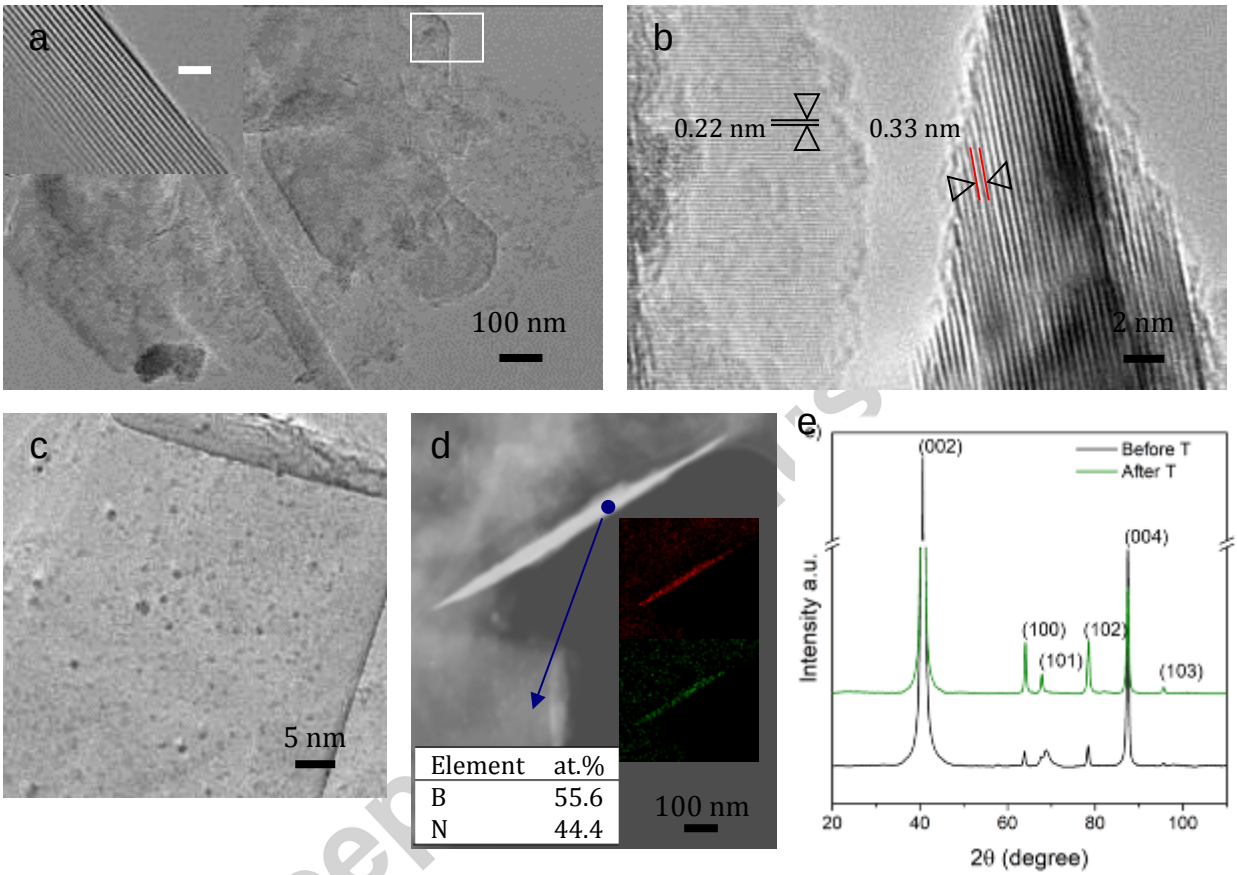

Fig. 3. TEM (a, c), high-resolution TEM (inset in (a) and (b)), SEM (d) micrographs and XRD patterns of BNNSs exfoliated from BN particles during ball milling before and after annealing at 100 ^{o}C (e). Insets in (d) show Nitrogen and Boron spatially-resolved EDS maps and elemental composition of BNNS in the area indicated by blue circle.

3.3. Microstructure of Al-BNNSs composites

The ball milled BNNSs were utilized as a reinforcement component in the Al/BN composites with 1, 5 and 10 wt.% of BNNSs. Microstructures of the sintered samples are presented in Fig. 4. Al/BN composites revealed BN layers along Al grain boundaries. For samples with 1 and 5 wt.% of BN phase, the maximum thickness of BN layers was below 1 μm but reached 2 μm for the composites with the highest BN content of 10 wt.%. Since the thickness

ACCEPTED MANUSCRIPT

of individual BNNSs after ball milling was about 20-50 nm, it becomes clear that the BN layers were formed by several agglomerated nanosheets.

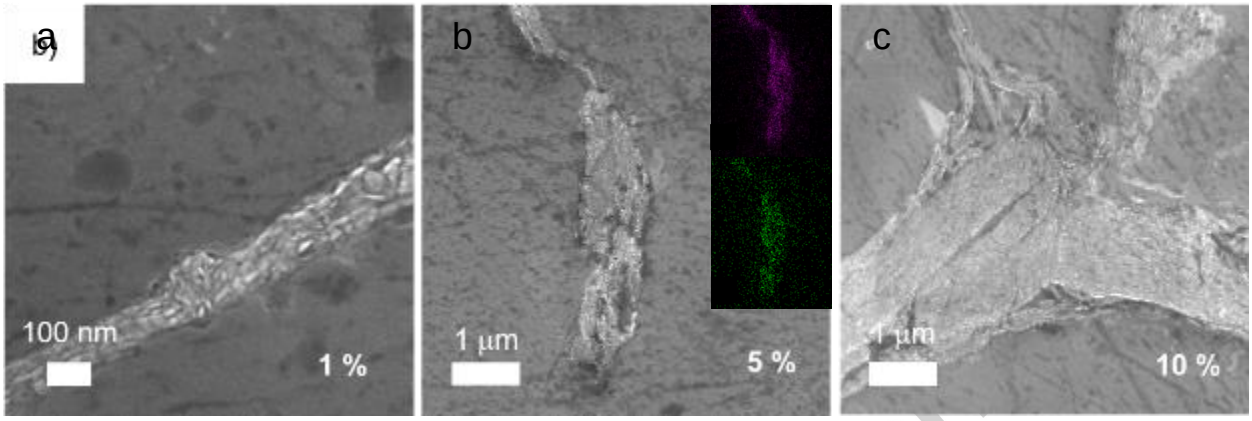

Fig. 4. SEM images and spatially-resolved Nitrogen and Boron EDX maps (insets in (b)) of Al-BNNSs composites with 1 (a), 5 (b) and 10 wt.% of BN phase (c).

Figure 5 shows the microstructures of an Al-1%BNNSs composite. It can be seen that the material consists of Al grains separated by BN layers, approximately 20-100 nm thick (Fig. 5a). Within these layers, individual *h*-BN nanosheets, about 5-10 nm thick and up to 200 nm long, are mostly oriented parallel to the Al grain boundaries. This minimizes the resistance to shear stress. Also, in some parts of the *h*-BN layers, the TEM image revealed numerous FeO_x NPs homogeneously distributed inside the BN phase (Fig. 5b). Thus, the Al grains were surrounded by a reinforcing frame consisting of a mixture of BNNSs with or without FeO_x NPs. Although oxide NPs can make an additional contribution to the layer strength, the likelihood of this is relatively low as these NPs were observed not within all BN layers. Note that the BN surface was perfectly wetted by molten Al because no detachments or delaminations were observed between the two phases. The composition maps revealed two features of Al grains: a significant amount of oxygen at the Al sub-grain boundaries and rare Fe-based inclusions, 0.5-2 μm in size, that appeare inside the Al grains during ball milling (Fig. 5e). The oxygen signal was observed to come from the oxide layers located at the Al sub-grains. No such oxygen signal was detected when BN layers were formed between Al grains hereby indicating a certain chemical interaction between neighboring phases. The XRD patterns of Al/BNNSs composites with different amounts of the reinforcing BN phase are depicted in Fig. 5f (PDF2: 11176). According to the XRD and

Accepted manuscript

TEM results, no additional phases, such as AlN or AlB_2 previously reported [29], formed in the Al-BNNSs composites.

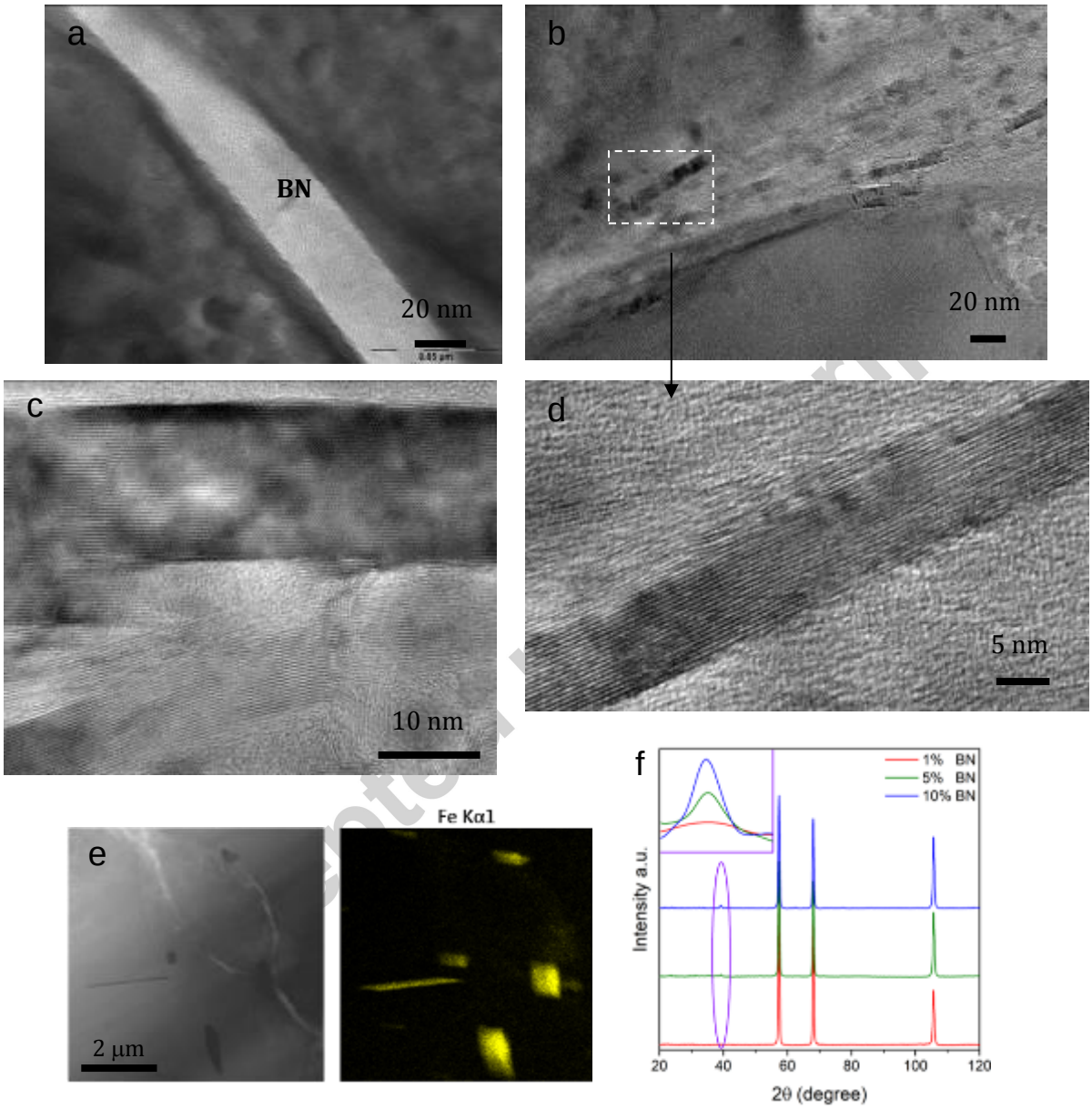

Fig. 5. TEM micrographs (a-d), SEM image and corresponding Fe EDS map (e) and XRD patterns of Al-BNNPs composites with 1, 5, and 10 wt.% of BN phase (f). Inset in (f) shows a close-up of the marked region of the XRD spectra.

3.4 Mechanical properties

Figure 6 shows the typical stress-strain curves for Al-BNNSs composites and the relationship between the room temperature tensile strength and BNNSs content. The maximum tensile strength of 152 MPa was obtained for a sample with 1 wt.% of BNNSs. A substantial increase in strength (69% increase compared with a 90 MPa value for pristine Al) can be attributed to the reinforcing role of BNNSs. Importantly, the Al-1%BNNSs sample demonstrated a high ductility, as evidenced by the shape of stress-strain curve. Note for comparison, that adding 1wt.% of BN nanotubes (BNNTs) into Al-based composites did not lead to a noticeable improvement in mechanical properties as compared to pristine Al [30, 31]. Thus our results are in contradiction with earlier conclusion drawn in relation to BNNTs that low BN contents (e.g., 1wt.%) are not fully able to significantly modify the composite performance in tension [30]. It is also worth noting that only 50% of improvement was previously reported for Al-based composites reinforced with BN nanoparticles although at much higher BN content (4.5 wt.%) [19]. Further increase in BNNSs content to 5 wt.% led to a dramatic decrease of tensile strength values down to 100 MPa. The Al-BNNSs with 10 wt.% of BN phase demonstrated extremely poor mechanical properties, even worse than those of pristine Al. This can be explained by too thick of BNNS layers located along the Al grain boundaries. These became stress concentrators.

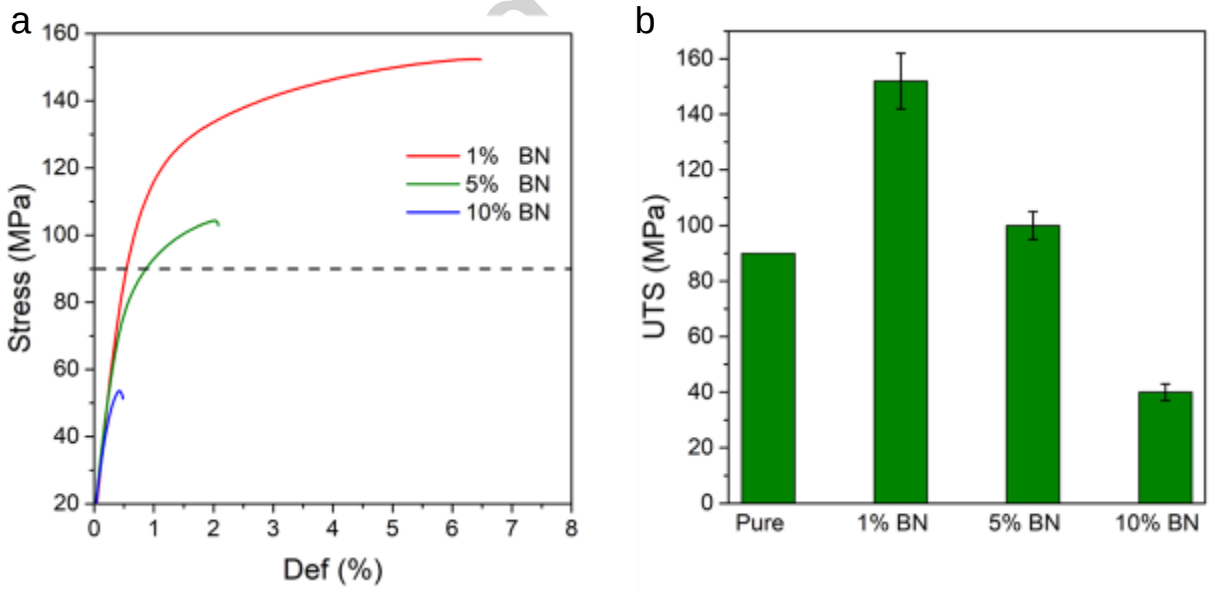

Fig. 6. Representative stress-strain curves (a) and tensile strength histogram of pure Al and Al/BNNSs composites with a different amount of the reinforcing BN phase (b).

ACCEPTED MANUSCRIPT

The superior mechanical properties of Al/BNNSs composites with only 1 wt.% of reinforcing phase can be attributed to a strong Al/BN interface and the relatively thin BN layers composed of BNNSs oriented in-parallel to the Al grain boundaries. Theoretical calculations predicted that the critical shear stress, which is one of the most important mechanical characteristics of composite, depends on the presence of defects [21] and the width of reinforcing nanoribbons [20]. The presence of vacancies give rise to an increase in critical shear strength. The decrease in the nanoribbon width leads to not only the increase of binding energy, but also to the increase of critical shear stress. In addition, the presence of chemically active edges significantly increases the critical shear stress values. Note, however, that even in the best sample with the highest strength (1 wt.% of BN), BNNSs were observed to form agglomerates (Fig. S2). This can lead to the partial deterioration of mechanical strength. This assumption is further confirmed by the observed significant decrease in composite strength of Al-BNNSs samples with high BN content. As it follows from the SEM and TEM data, the BNNSs frame thickness in the Al-1%BNNSs sample varies widely from 20 nm to 1 μm. It is clear that large thickness of BNNSs interlayer weakens the interface strength. Thus further fine tuning of the composite structure is required to achieve even better mechanical properties.

3.5 Microstructure of Al-BNNSs fracture surface

To shed the light on the mechanism of deformation and fracture, samples after tensile tests were characterized by SEM. The typical SEM micrographs of the fracture surfaces of the Al-BNNSs composites with 1 and 5 wt.% of BN are depicted in Fig. 7. Notably, the Al grains and BN layers have a strong cohesion to each other. BNNSs are seen to be firmly adjacent to the metal matrix. In addition, Al grains with no signs of local plastic deformation, which is usually characterized by a peculiar dimpling structure [29], were observed. This suggests that the BNNSs were indeed involved in the deformation process and took over most part of the load. Note that the orientation of BNNSs relative to the applied load is critical in terms of their contribution to hardening. In the case when the BNNSs are oriented roughly perpendicular to the applied load (see Fig. 7a and b), they can make a significant contribution to the tensile strength. The brittle fracture of the BNNSs supports this conclusion (see double arrows in Fig. 7a and b). When a load is applied parallel to the Al/BN interface, a grain boundary sliding between BNNSs

Accepted manuscript

can be expected. Since both types of interfaces are randomly distributed in the Al-BNNSs composites relative to an applied load, it is reasonable to expect that both the strength and ductility may be improved.

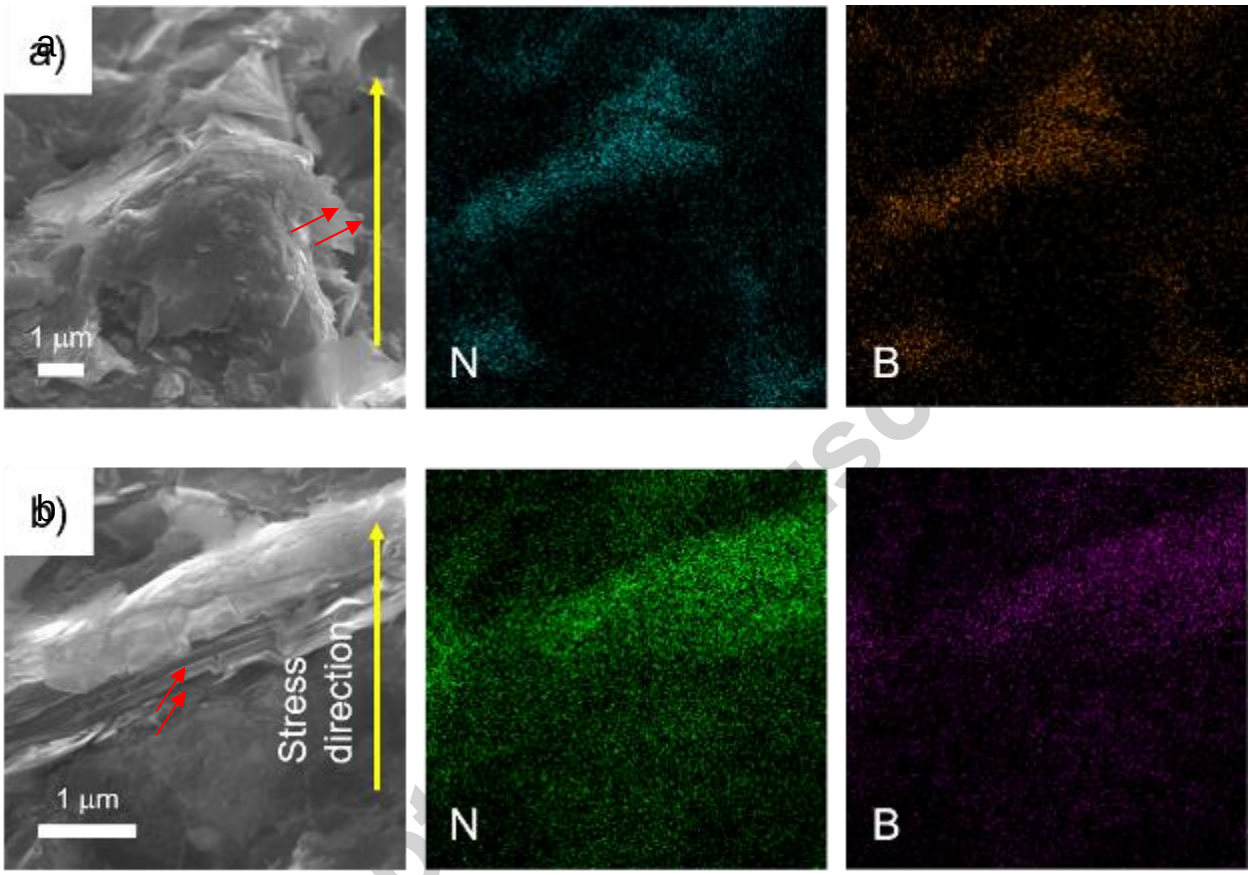

Fig. 7. SEM images illustrating fracture surface of Al-BNNSs composite with 1 (a) and 5 wt.% of BN phase (b) and corresponding spatially-resolved Nitrogen and Boron EDS maps.

In order to better understand the contribution of BNNSs to the material strength, a sample with 1wt.% of BN phase was thoroughly analyzed by high-resolution TEM. Figure 8 illustrates the structure of the SPS-produced Al-BNNSs composite near its fractured area after the tensile test at room temperature. The distinguished feature of the sample is the structural evidence of BNNSs in carrying the tensile load. The image in Fig. 8a displays BNNSs which turned out to be severely deformed. One of the nanoribbons (shown by the double arrow) was bent, but its basic planes did not break. Other BN nanoplate is seen to be bent and partially broken in two places (shown by single arrows) due to multidirectional local loading. These results indicate that the

ACCEPTED MANUSCRIPT

material structure was indeed severely loaded during a tensile test and the BN nanoribbons took over most portion of the load. An interesting observation is that the Al/BN interface was strong enough to withstand the applied load because no detachment or delamination was observed (Fig. 8b). Thus, BNNSs located between the Al grains cemented the whole structure, just in accordance with the experimentally observed drastic increase in Al-BNNSs strength.

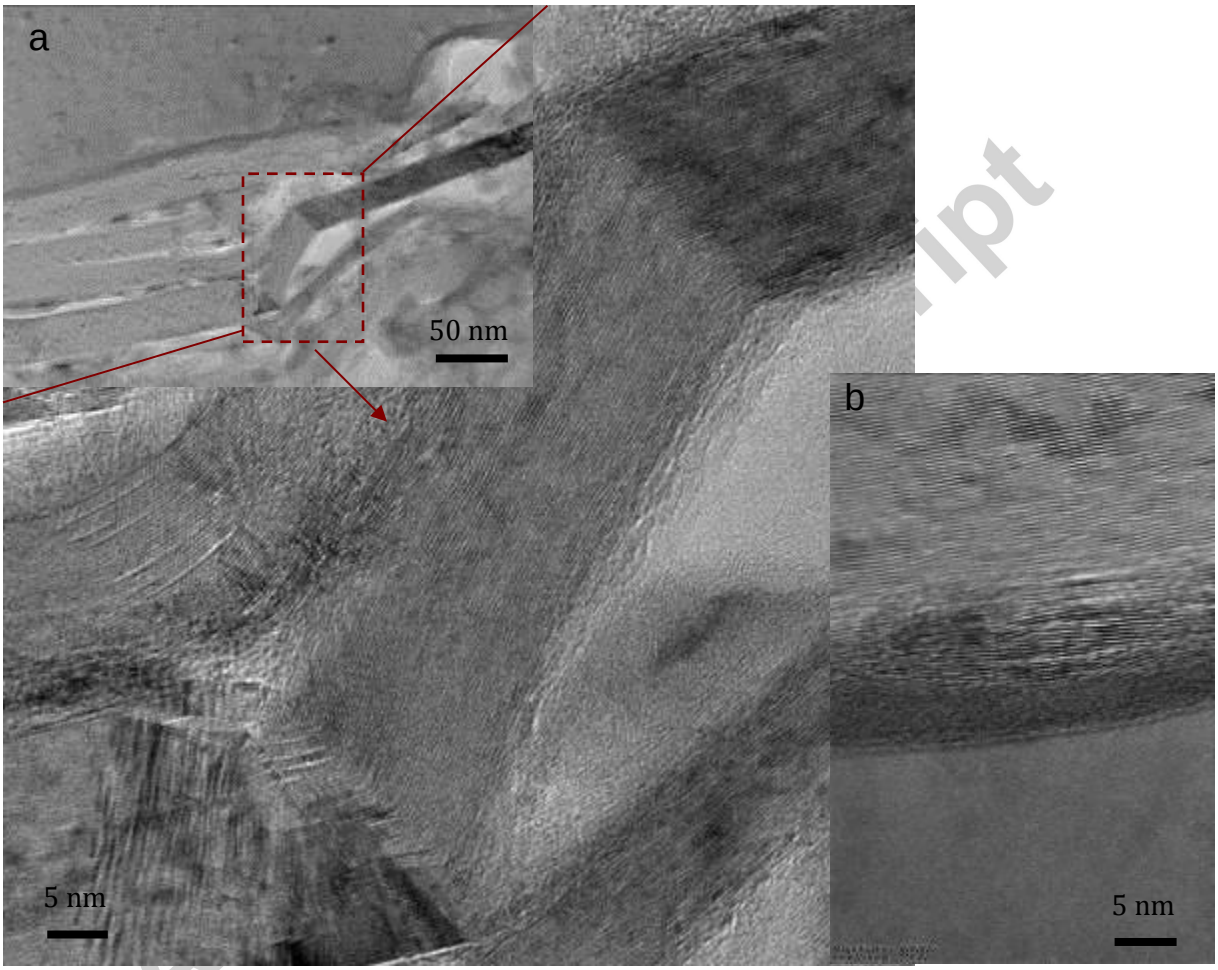

Fig. 8. TEM images of an Al-1%BNNPs composite after the tensile test.

4. Conclusions

BN nanosheets (BNNSs) exfoliated by ball milling in liquid from commercially available *h*-BN particles, 7-15 μm in size, were utilized to fabricate Al-BNNSs composites with 1, 5 and 10 wt.% of BN phase using spark plasma sintering. To establish the optimal ball milling mode

ACCEPTED MANUSCRIPT

(i.e. to achieve high yield of high-quality BNNSs with minimal processing time) the following parameters were adjusted: milling time (20 - 240 min), processing media (Ar, isopropanol, ethylene glycol), media to BN powder weight ratio (1:1 and 2:1), as well as size and ratio of balls (a mixture of balls with a diameter of 5, 7 and 9 mm in equal proportion or balls of a specific diameter (5, 7 or 9 mm) were used). The results indicated that the ball milling process was highly efficient, took only 20 min and allowed one to obtain high yield of uniform and not deformed BNNSs with an average size of 300×600 nm^2 and a thickness of approximately 20-50 nm. Some BNNSs contained FeO_x nanoparticles as a by-product of ball milling process. The BNNSs formed layers (whose thickness varied from 20 nm to 1-2 μm depending on the BNNSs content) between Al grains in which they were mostly oriented parallel to the Al grain boundaries. The maximum tensile strength of 152 MPa was obtained for a sample with 1 wt.% of BNNSs indicating 69% increment compared to pristine Al. Detailed structural investigation of the fractured surfaces confirmed that (i) the BNNSs were severely deformed and therefore were heavily involved in the deformation process, (ii) took over most part of the tensile load, and (iii) Al/BN interface was strong enough to withstand the applied load. The present and previously obtained theoretical results clearly demonstrate that BNNSs are one of the most promising fillers for the improvement of Al mechanical properties. However, additional efforts are needed to achieve a more homogeneous distribution of BNNSs along the Al grain boundaries.

Acknowledgements

This work was supported by the Ministry of Education and Science of the Russian Federation (State task No. 11.937.2017/ПЧ. S.C. thanks Increase Competitiveness Program of NUST "MISiS" (No. K2-2018-013)). D.V.G. particularly acknowledges the Australian Research Council (ARC) for granting an Australian Laureate Fellowship (FL160100089).

Notes

Declarations of interest: none

Appendix A. Supporting information

Supplementary data associated with this article can be found in the online version at …….

Accepted manuscript

ACCEPTED MANUSCRIPT

References

[1] A. Saxena, N. Singh, D. Kumar, P. Gupta, Effect of ceramic reinforcement on the properties of metal matrix nanocomposites, Mater. Today Proc. 4 (2017) 5561–5570. doi:10.1016/J.MATPR.2017.06.013.

[2] H. Ye, X.Y. Liu, H. Hong, Fabrication of metal matrix composites by metal injection molding - A review, J. Mater. Process. Technol. 200 (2008) 12–24. doi:10.1016/J.JMATPROTEC.2007.10.066.

[3] K. Shirvanimoghaddam, S.U. Hamim, M. Karbalaei Akbari, S.M. Fakhrhoseini, H. Khayyam, A.H. Pakseresht, E. Ghasali, M. Zabet, K.S. Munir, S. Jia, J.P. Davim, M. Naebe, Carbon fiber reinforced metal matrix composites: Fabrication processes and properties, Compos. Part A 92 (2017) 70–96. doi:10.1016/J.COMPOSITESA.2016.10.032.

[4] Y.X. Gan, J. Dong, J.B. Gan, Carbon network/aluminum composite made by powder metallurgy and its corrosion behavior in seawater, Mater. Chem. Phys. 202 (2017) 190–196. doi:10.1016/J.MATCHEMPHYS.2017.09.033.

[5] T. Ghrib, Structural, optical and thermal properties of nanoporous aluminum, Thermochim. Acta. 599 (2015) 57–62. doi:10.1016/J.TCA.2014.11.020.

[6] A. Maleki, A.R. Taherizadeh, H.K. Issa, B. Niroumand, A.R. Allafchian, A. Ghaei, Development of a new magnetic aluminum matrix nanocomposite, Ceram. Int. 44 (2018) 15079–15085. doi:10.1016/J.CERAMINT.2018.05.141.

[7] S. Correia, V. Anes, L. Reis, Effect of surface treatment on adhesively bonded aluminium-aluminium joints regarding aeronautical structures, Eng. Fail. Anal. 84 (2018) 34–45. doi:10.1016/J.ENGFAILANAL.2017.10.010.

[8] S.V. Prasad, R. Asthana, Aluminum metal–matrix composites for automotive applications: tribological considerations, Tribol. Lett. 17 (2004) 445–453. doi:10.1023/B:TRIL.0000044492.91991.f3.

[9] S.P. Rawal, Metal-matrix composites for space applications, JOM 53 (2001) 14–17. doi:10.1007/s11837-001-0139-z.

[10] I.J. Polmear, Light alloys : metallurgy of the light metals, New York, 1995.

Accepted manuscript

ACCEPTED MANUSCRIPT

[11] H. Zare, M. Jahedi, M.R. Toroghinejad, M. Meratian, M. Knezevic, Compressive, shear, and fracture behavior of CNT reinforced Al matrix composites manufactured by severe plastic deformation, Mater. Des. 106 (2016) 112–119. doi:10.1016/J.MATDES.2016.05.109.

[12] L. Yuan, J. Han, J. Liu, Z. Jiang, Mechanical properties and tribological behavior of aluminum matrix composites reinforced with in-situ AlB_2 particles, Tribol. Int. 98 (2016) 41–47. doi:10.1016/J.TRIBOINT.2016.01.046.

[13] J. Wang, Z. Li, G. Fan, H. Pan, Z. Chen, D. Zhang, Reinforcement with graphene nanosheets in aluminum matrix composites, Scr. Mater. 66 (2012) 594–597. doi:10.1016/J.SCRIPTAMAT.2012.01.012.

[14] Q. Yang, Y. Zhang, H. Zhang, R. Zheng, W. Xiao, C. Ma, Fabrication of Al-based composites reinforced with in situ devitrified $Al_{84}Ni_{8.4}Y_{4.8}La_{1.8}Co_1$ particles by hot pressing consolidation, J. Alloys Compd. 648 (2015) 382–388. doi:10.1016/J.JALLCOM.2015.07.011.

[15] D. Markó, K.G. Prashanth, S. Scudino, Z. Wang, N. Ellendt, V. Uhlenwinkel, J. Eckert, Al-based metal matrix composites reinforced with $Fe_{49.9}Co_{35.1}Nb_{7.7}B_{4.5}Si_{2.8}$ glassy powder: Mechanical behavior under tensile loading, J. Alloys Compd. 615 (2014) S382–S385. doi:10.1016/J.JALLCOM.2013.10.215.

[16] S. Khoramkhorshid, M. Alizadeh, A.H. Taghvaei, S. Scudino, Microstructure and mechanical properties of Al-based metal matrix composites reinforced with $Al_{84}Gd_6Ni_7Co_3$ glassy particles produced by accumulative roll bonding, Mater. Des. 90 (2016) 137–144. doi:10.1016/J.MATDES.2015.10.063.

[17] L. Zhang, H. Xu, Z. Wang, Q. Li, J. Wu, Mechanical properties and corrosion behavior of Al/SiC composites, J. Alloys Compd. 678 (2016) 23–30. doi:10.1016/J.JALLCOM.2016.03.180.

[18] M. Yamaguchi, J. Bernhardt, K. Faerstein, D. Shtansky, Y. Bando, I.S. Golovin, H.-R. Sinning, D. Golberg, Fabrication and characteristics of melt-spun Al ribbons reinforced with nano/micro-BN phases, Acta Mater. 61 (2013) 7604–7615. doi:10.1016/J.ACTAMAT.2013.08.062.

[19] K.L. Firestein, A.E. Steinman, I.S. Golovin, J. Cifre, E.A. Obraztsova, A.T. Matveev, A.M. Kovalskii, O.I. Lebedev, D. V. Shtansky, D. Golberg, Fabrication, characterization,

Accepted manuscript

ACCEPTED MANUSCRIPT

and mechanical properties of spark plasma sintered Al–BN nanoparticle composites, Mater. Sci. Eng. A 642 (2015) 104–112. doi:10.1016/J.MSEA.2015.06.059.

[20] D.G. Kvashnin, M. Ghorbani-Asl, D. V. Shtansky, D. Golberg, A. V. Krasheninnikov, P.B. Sorokin, Mechanical properties and current-carrying capacity of Al reinforced with graphene/BN nanoribbons: a computational study, Nanoscale 8 (2016) 20080–20089. doi:10.1039/C6NR07206B.

[21] A. V. Krasheninnikov, N. Berseneva, D.G. Kvashnin, J. Enkovaara, T. Björkman, P. Sorokin, D. Shtansky, R.M. Nieminen, D. Golberg, Toward stronger Al–BN nanotube composite materials: Insights into bonding at the Al/BN interface from first-principles calculations, J. Phys. Chem. C. 118 (2014) 26894–26901. doi:10.1021/jp509505j.

[22] Y. Chen, H. Liang, Q. Abbas, J. Liu, J. Shi, X. Xia, H. Zhang, G. Du, Growth and characterization of porous sp^2-BN films with hollow spheres under hydrogen etching effect via borazane thermal CVD, Appl. Surf. Sci. 452 (2018) 314–321. doi:10.1016/J.APSUSC.2018.04.217.

[23] J. Xiong, J. Luo, L. Yang, J. Pang, W. Zhu, H. Li, Boron defect engineering in boron nitride nanosheets with improved adsorptive desulfurization performance, J. Ind. Eng. Chem. 64 (2018) 383–389. doi:10.1016/J.JIEC.2018.04.001.

[24] Y. Zhan, J. Yan, M. Wu, L. Guo, Z. Lin, B. Qiu, G. Chen, K. Wong, Boron nitride nanosheets as a platform for fluorescence sensing, Talanta 174 (2017) 365–371. doi:10.1016/J.TALANTA.2017.06.032.

[25] M. Nasr, L. Soussan, R. Viter, C. Eid, R. Habchi, P. Miele, M. Bechelany, High photodegradation and antibacterial activity of BN–Ag/TiO_2 composite nanofibers under visible light, New J. Chem. 42 (2018) 1250–1259. doi:10.1039/C7NJ03183A.

[26] Deepika, L.H. Li, A.M. Glushenkov, S.K. Hait, P. Hodgson, Y. Chen, High-efficient production of boron nitride nanosheets via an optimized ball milling process for lubrication in oil, Sci. Rep. 4 (2015) 7288. doi:10.1038/srep07288.

[27] K.M. Kabezya, H. Motjotji, The effect of ball size diameter on milling performance, J. Mater. Sci. Eng. 4 (2014) 1–3. doi:10.4172/2169-0022.1000149.

[28] J. Kim, S. Lee, Y.R. Uhm, J. Jun, C.K. Rhee, G.M. Kim, Synthesis and growth of boron nitride nanotubes by a ball milling–annealing process, Acta Mater. 59 (2011) 2807–2813. doi:10.1016/J.ACTAMAT.2011.01.019.

Accepted manuscript

ACCEPTED MANUSCRIPT

[29] A.E. Steinman, S. Corthay, K.L. Firestein, D.G. Kvashnin, A.M. Kovalskii, A.T. Matveev, P.B. Sorokin, D. V. Golberg, D. V. Shtansky, Al-based composites reinforced with AlB_2, AlN and BN phases: Experimental and theoretical studies, Mater. Des. 141 (2018) 88–98. doi:10.1016/J.MATDES.2017.12.022.

[30] M. Yamaguchi, F. Meng, K. Firestein, K. Tsuchiya, D. Golberg, Powder metallurgy routes toward aluminum boron nitride nanotube composites, their morphologies, structures and mechanical properties, Mater. Sci. Eng. A. 604 (2014) 9–17. doi:10.1016/J.MSEA.2014.02.086.

[31] Y. Xue, B. Jiang, L. Bourgeois, P. Dai, M. Mitome, C. Zhang, M. Yamaguchi, A. Matveev, C. Tang, Y. Bando, K. Tsuchiya, D. Golberg, Aluminum matrix composites reinforced with multi-walled boron nitride nanotubes fabricated by a high-pressure torsion technique, Mater. Des. 88 (2015) 451–460. doi:10.1016/J.MATDES.2015.08.162.

Accepted manuscript